ACS APPLIED BIO MATERIALS

www.acsabm.org Article

Morphology-Dependent Performance of MnO_2 Nanostructure–Carbon Dot-Based Biosensors for the Detection of Glutathione

Neeraj Sohal, Banibrata Maity,* and Soumen Basu*

Cite This: *ACS Appl. Bio Mater.* 2021, 4, 5158–5168 Read Online

ACCESS | Metrics & More | Article Recommendations | Supporting Information

ABSTRACT: Herein, we develop a facile, sensitive, and selective fluorescent nanosensor for the detection of glutathione (GSH). In this protocol, carbon dots (Cdots) with a fairly high quantum yield were synthesized by a microwave-assisted pyrolysis technique. Moreover, different shapes of the MnO_2 nanostructure were also prepared by the hydrothermal technique. A comparative photophysical study of different morphology-dependent Cdots@MnO_2 nanostructure-based biosensors was explored, which showed different results for the quenching values of ("turn-off") fluorescence intensity, quantum yields, electron transfer rate, and average lifetime. The structure, property, and performance of nanomaterials are interdependent. Therefore, the different shapes of MnO_2, that is, nanoflowers (NFs), nanorods (NRs), and a mixture of NFs/NRs was prepared by the hydrothermal method owing to different specific surface areas (23–69 $m^2\ g^{-1}$) which put the impact on their sensing activity. It was observed that the variation in the different photophysical parameters of fluorescent Cdots such as quantum yield (Φ), average lifetime values [τ_{av} (ns)], radiative (k_r) rate constant, nonradiative (k_{nr}) rate constant, rate of electron transfer (k_{ET}), the efficiency of electron transfer (Φ_{EET}), FRET efficiency (E), and Förster distance (R_0) were dependent on the different shapes of the MnO_2 nanostructure. These results indicate that the transfer of energy occurs between the Cdots and different shapes of MnO_2 nanostructures based on fluorescence resonance energy transfer at different charge-transfer rates. The recovery rate ("turn-on") of fluorescence of Cdots with the addition of GSH was obtained best for the NF structure by conversion of MnO_2 to Mn^{2+}, and the limit of detection was obtained as ~19 μM for GSH. The developed sensing probes were rapid, easy, cheap, and eco-friendly for the determination of GSH.

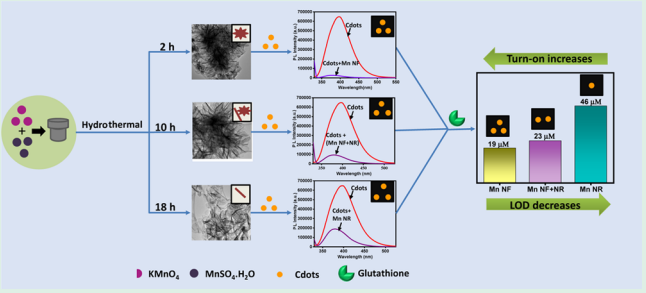

KEYWORDS: *biosensor, carbon dots, MnO_2 nanostructure, glutathione, fluorescence sensing*

INTRODUCTION

Glutathione (GSH) is one of the rich small molecular biothiols, which plays a vital role in the human physiology system.[1] GSH is also regarded as a tripeptide, which consists of glycine, L-cysteine, and L-glutamic acid. GSH provides significant contribution in physiological and pathological events like cellular redox homeostasis, growing tissues, regulation of the human metabolism, gene regulation, and detoxification.[2,3] Moreover, it helps in the modulation of cell proliferation by shielding the cells from the effect of oxidative stress and trapping the free radicals to avoid the injury of DNA and RNA.[4] The abnormal level of GSH is directly related to causing different diseases including HIV, AIDS, aging, cancer, Parkinson's, cardiovascular disease, and autism in children.[5] Therefore, the development and detection methods of GSH in living cells have attracted a great deal of considerable attention. In the present time, the different methods have been reported for the detection of GSH, including electrochemistry, high-performance liquid chromatography, chemiluminescence, colorimetry, photoelectrochemistry, mass spectrometry, surface-enhanced Raman scattering, enzyme-linked immunosorbent assay, fluorescence spectroscopy, and so forth.[4] These techniques limit their practical applications due to time consumption, expensive instrumentation, and less sensitive and tricky handling nature. The fluorescence spectroscopy method draws considerable attention compared with other instrumental techniques due to its significant advantages of simplicity, nondestructive properties, and high sensitivity.[6] As a result, great exertions have been devoted to develop the high fluorescence sensing platforms for the ultrasensitive detection of GSH.

Fluorescent carbon dots (Cdots) are luminescent nanomaterials having sizes of 1–10 nm.[7,8] Cdots are an excellent alternative to organic fluorescent dyes, upconversion nanoparticles, and other quantum dots to act as biosensing and

Received: March 23, 2021
Accepted: May 11, 2021
Published: May 26, 2021

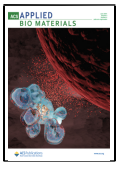

https://doi.org/10.1021/acsabm.1c00353
ACS Appl. Bio Mater. 2021, 4, 5158–5168

bioimaging agents due to their extraordinary properties such as low toxicity, exceptional biocompatibility, great photostability, the easy preparation method, and so forth.[9,10] There are different synthetic approaches to prepare fluorescent Cdots, such as hydrothermal treatment, the solvothermal method, electrochemical treatment, microwave treatment, ultrasonication, normal heating, the arc discharge method, laser ablation, chemical oxidation, and so forth.[11,12] Recently, various fluorescence sensing platforms have been developed for the detection of GSH. These fluorescence sensing platforms are based on the different quenching mechanisms which include fluorescence resonance energy transfer (FRET), photoinduced electron transfer (PET), static or dynamic quenching, the inner filter effect, and many others through fluorophore−quencher pairs.[13]

Manganese oxide (MnO_2) has become an active material in the field of biosensing among different transition-metal oxides due to its attractive physical and electrochemical properties.[14] MnO_2 has exceptional light absorption capability, a high surface area, and a rapid rate of electron transfer due to which it can be used as a proficient fluorescence quencher in developing a "turn-off-on" sensing platform.[15,16] The properties of nanomaterials can be tuned by controlling their size, shape, crystallographic orientation, and morphology.[17,18] Shape control becomes the most important technique for improving the activity of nanomaterials.[19] An interdependent relationship has been observed between the structure, property, and performance of nanomaterials.[20] Currently, a variety of approaches (e.g., solid-state, refluxing, hydrothermal treatment, and sol−gel) have been reported for the preparation of different-shaped MnO_2 nanostructures along with their changed crystal structures from either the reduction of MnO_4^- or oxidation of Mn^{2+}.[21] Different kinds of reaction conditions like pH, concentrations of the substrate, temperature, reactants, counter cations, and anions are also responsible for the variation of different morphologies of nanostructures and their crystalline phases.[22] The different shapes of MnO_2 nanostructures can be synthesized, which include nanorods (NRs), nanowires (NWs), nanotubes (NTs), nanosheets (NSs), nanoflowers (NFs), and nanospheres (NSPs), and their catalytic properties get significantly altered by the variation of their shape or morphology.[19,20] MnO_2 nanostructures have many applications due to versatility in structures, various oxidation states like +2, +3, or +4 of Mn, and 2 or 3 valence states present in a similar crystal structure.[23] The morphology of the nanostructure and the active sites present on the surface of MnO_2 provides significant contribution in the sensing performance of materials.[24] MnO_2 consists of five different polymorphs, which include α, β, γ, δ, and ε, which are further interconnected through the elementary unit of the [MnO_6] octahedron by an edge or corner sharing due to the fact that they have exceptional properties.[24−26] Wu et al.[19] synthesized MnO_2 nanoparticles of different morphologies such as NWs, NRs, and NTs. They found that the sensing activity was dependent on the different shapes or morphologies of MnO_2 nanoparticles. Peng et al.[27] prepared the SiO_2@MnO_2 nanocomposite as an immunochromatography sensing probe for the detection of antibiotics and GSH. They found that the addition of GSH in the fluorescent nanoprobe leads to quenching of fluorescence intensity due to the conversion of the oxidation state of MnO_2(IV) to Mn(II) species. Li et al.[28] developed a biosensor based on the MnO_2−Cu nanocluster fluorescence sensing platform for the detection of GSH. They examined that Cu nanoclusters in the sensing probe play roles both as an energy donor and a signal enhancer, while MnO_2 NSPs serve as an energy acceptor as well as a recognizer. Recently, we have developed a fluorescent nanoprobe that consists of Cdots and different-size MnO_2 NSPs for ultrasensitive detection of GSH.[29] We studied the different photophysical parameters such as quantum yield, average lifetime values, radiative rate constant, nonradiative rate constant, rate of electron transfer, the efficiency of electron transfer, FRET efficiency, and Förster distance. We also determined the photoluminescence (PL) properties of Cdots and found that the variation in size affects the performance of MnO_2 in the sensing ability of GSH.

In this study, we have used ascorbic acid (carbon precursor) for the preparation of Cdots through a one-pot microwave-assisted method.[16] Also, we have also prepared different shapes of MnO_2 nanostructures via an optimized hydrothermal method.[30] Three different shapes of MnO_2 nanostructures, that is, NF, NF + NR, and NR, were synthesized and characterized by transmission electron microscopy (TEM) analysis. The nanocomposites of Cdots with MnO_2 nanostructures were prepared by mixing the two solutions with sonication. The synthesized different-shape Cdot-MnO_2 nanostructures act as turn-off sensors with PL quenching. Furthermore, the GSH sensing was studied in the presence of synthesized various shapes of Cdot-MnO_2 nanostructures which were rationalized as a turn-on sensor with an enhancement of the fluorescence. A redox reaction would occur among MnO_2 and GSH in the presence of GSH in the Cdot-MnO_2 sensing solution. This redox reaction increases the fluorescence of Cdots by the conversion of MnO_2 to Mn^{2+} ions, and GSH gets oxidized to GSH disulfide through a thiol−disulfide exchange reaction.[31] The different shapes of the MnO_2 nanostructure had a great impact on their interaction with Cdots and GSH. Also, we found that the variation in the shape of the MnO_2 nanostructure modulates the sensitivity of GSH.

MATERIALS AND REAGENTS

Hydrated manganese sulfate ($MnSO_4·H_2O$) (99%) and potassium permanganate ($KMnO_4$) (99%) were bought from Loba Chemie, India. These chemicals were used to prepare different morphologies of MnO_2 nanostructures. Ascorbic acid (99%) was bought from Loba Chemie and used as a carbon source, and Kollicoat-IR (MW 45,000 Da) was gifted by BASF and was used as a precursor stabilizing agent for the synthesis of Cdots. L-GSH was purchased from Hi-media and was further used as received without any purification for sensing. Ultrapure deionized (DI) water was prepared by a double-distillation unit and further used for preparing all stock solutions.

Method for Preparation of Cdots. First, ascorbic acid (0.1 M) and Kollicoat (0.1 M) were dissolved in DI water by continuous stirring for 30 min. Further, the clear mixture was transferred to a glass reaction vial, and it was heated at 130 °C for 30 min by using a Multiwave-300 microwave reaction system (300 W) (Anton Paar, USA). The color change of the mixture from colorless to pale yellow signified the final preparation of Cdots.[16,29]

Method for Preparation of Different Shapes of the MnO_2 Nanostructure. Different shapes of the MnO_2 nanostructure were synthesized by using $MnSO_4·H_2O$ and $KMnO_4$ solutions through the hydrothermal method. Further, 0.2 and 0.5 g of $MnSO_4·H_2O$ and $KMnO_4$, respectively, were well mixed in 100 mL of DI water. The dissolved solution of $KMnO_4$ and $MnSO_4$ was transferred into a Teflon-lined pressure vial and then put into an oven preheated to 140 °C for three different dwell times, that is, 2, 10, and 18 h (Scheme 1). The pressure vial was cooled down to normal temperature with the

https://doi.org/10.1021/acsabm.1c00353
ACS Appl. Bio Mater. 2021, 4, 5158−5168

Scheme 1. Schematic Illustration of the Synthesis of Different Shapes of MnO_2 Nanostructures

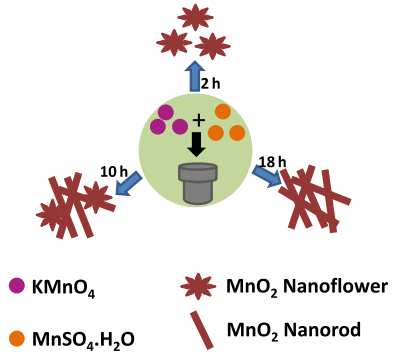

completion of the reaction. The precipitates of MnO_2 formed were further washed with DI water so that the pH of the supernatant becomes neutral, and at last, MnO_2 precipitates were dried at 100 °C.[30] According to their morphology, the MnO_2 nanostructures were named Mn NF, Mn NF + NR, and Mn NR for the dwell times of 2, 10, and 18 h, respectively.

Characterization. Absorption and emission spectra of Cdot-MnO_2 nanostructures were recorded via a UV−visible (UV−vis) spectrophotometer (Analytik Jena, Specord, India) and fluorescence spectrofluorimeter (PerkinElmer LS-55, USA). The different morphologies or shapes of the MnO_2 nanostructure were examined through transmission electron microscopy (TEM, FEI Tecnai G2 F20). The crystal structure of the synthesized MnO_2 nanostructure was examined by X-ray diffraction (XRD, PANalytical X'Pert PRO) with Cu Kα (λ = 1.540Å) as the radiation source ($0 \leq 2\theta \leq 90°$). The surface areas of the different morphologies of MnO_2 nanostructures were obtained via the Brunauer−Emmett−Teller (BET) surface area analyzer of BEL-miniII, Microtrac Corp. Pvt. Ltd., Japan.

Preparation of the Sample Solution of Cdots and the MnO_2 Nanostructure. The stock solutions of different shapes of the MnO_2 nanostructure of specific concentrations were prepared. The sensing solutions (Cdot-MnO_2 nanostructures) were formed by the addition of the respective shape of the MnO_2 nanostructure to the solution of Cdots in 2 mL of distilled water. The detection of GSH was evaluated by mixing different concentrations of GSH (0−150 μM) with Cdot-MnO_2 nanocomposites. The sample was further placed for the incubation time of 10 min. Finally, the solution was transferred to a 3 mL glass cuvette. The emission spectra of the prepared samples were excited at the excitation wavelength of 340 nm (λ_{exi} = 340 nm).

Measurement of Fluorescence Quantum Yield. The fluorescence quantum yields of Cdots in the presence of different shapes of MnO_2 nanostructures and GSH were evaluated with respect to quinine sulfate[32] (reference solution) having Φ_R = 0.546 by using the following equation:

$$\phi_S = \phi_R \times \frac{A_S}{A_R} \times \frac{(\mathrm{Abs})_R}{(\mathrm{Abs})_S} \times \frac{\eta_S^2}{\eta_R^2} \quad (1)$$

The subscripts "S" and "R" represent the sample and reference solution, respectively. "Φ_S" and "Φ_R" correspond to the fluorescence quantum yields of the sample and reference solution, respectively. "Abs", "A", and "η" refer to the absorbance, the area of fluorescence emission, and the refractive index, respectively.

RESULTS AND DISCUSSION

The crystal phase identification of MnO_2 nanostructures prepared at different dwell times was characterized by XRD analysis. The existence of a broad peak showed that the synthesized nanomaterials contain both amorphous and crystalline phases. Figure 1a shows that the crystallinity of the MnO_2 nanostructure increased with the increment in the dwell time from 2 to 18 h, that is, from NF to NR. The MnO_2 nanostructure prepared at 2 h (Mn NF), 10 h (Mn NF + NR), and 18 h (Mn NR) showed diffraction peaks at 2θ ~13°, ~26°, ~38°, and ~65° corresponding to the (110), (220), (211), and (002) lattice planes, respectively. It showed similarity to those of α-MnO_2 (ICDD-JCPDS no. 04−0141) with a tetragonal unit cell having lattice parameters of $a = b$ = 9.78 Å and c = 2.86 Å.[33] It was observed that with the increase of dwell time, the crystallinity of the nanostructure increases from Mn NF to Mn NR with the appearance of sharper and narrower peaks. The energy-dispersive X-ray spectroscopy (EDS) analysis also confirms the formation of the pure MnO_2 nanostructure without any impurities as shown in Figure 1b.

The morphology of the MnO_2 nanostructure prepared at 2, 10, and 18 h was observed as NF (Figure 2a), a mixture of NFs and NRs (Figure 2b), and only NRs (Figure 2c) by TEM analysis. It was found that the ratio of NFs to NRs and the crystalline nature of the MnO_2 nanostructure enhanced with an increment of the time duration of the reaction. Therefore, the final morphology formed of the MnO_2 nanostructures was strongly correlated with the dwell time. An average d-spacing, that is, 0.35 nm, was determined in the lattice-resolved high-resolution TEM (HR-TEM) images of MnO_2 NF (Figure 2d), MnO_2 NF + NR (Figure 2e), and MnO_2 NF (Figure 2f), which was indexed to the separation between (220) lattice planes.[30] It shows that all three different shapes of the MnO_2 nanostructure have the same d-spacing value and correspond

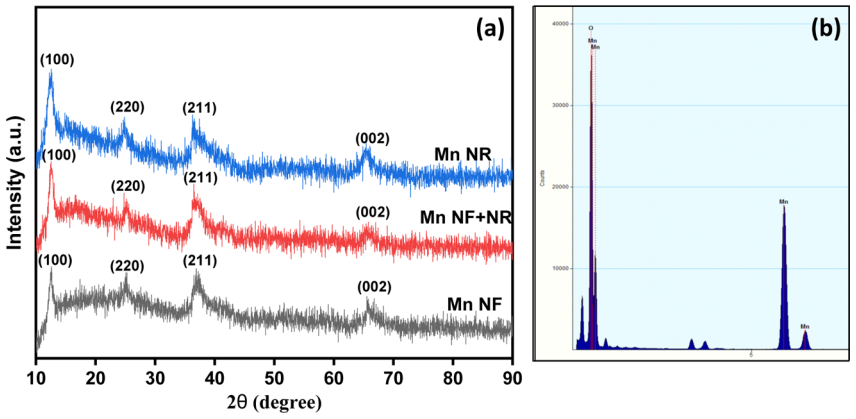

Figure 1. (a) XRD pattern of different MnO_2 nanostructures and (b) EDS spectra of MnO_2 NFs.

https://doi.org/10.1021/acsabm.1c00353
ACS Appl. Bio Mater. 2021, 4, 5158−5168

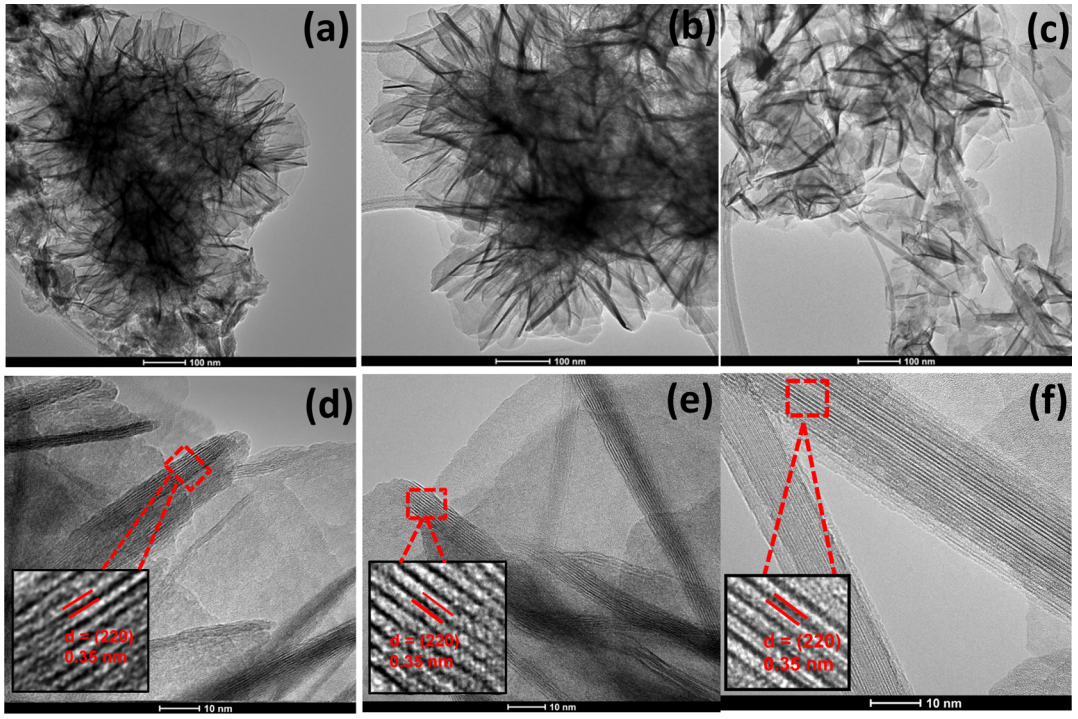

Figure 2. TEM and HR-TEM images with an inset image of a specific *d*-spacing value of (a,d) Mn NF, (b,e) Mn NF + NR, and (c,f) Mn NR.

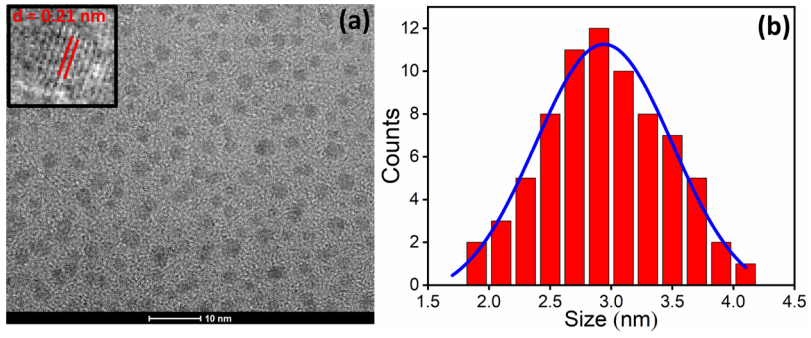

Figure 3. (a) HR-TEM image with an inset image of lattice fringes and (b) particle size distribution histogram of Cdots.

to (220) lattice planes. Figure 3a represents the HR-TEM image of Cdots having partially monodispersed and spherical particles. The inset image of Figure 3a shows lattice fringes with the *d*-spacing value of 0.21 nm corresponding to the (100) graphitic lattice plane.[29] Figure 3b shows the histogram distribution of Cdot particles with a narrow range (1.5−4 nm) and an average diameter of 2.9 nm.

The optical properties of Cdots and different shapes of the MnO_2 nanostructure were investigated by their UV−vis absorption spectra. We have already reported that Cdots show a sharp peak of absorption at 263 nm, which corresponds to $n-\pi^*$ and $\pi-\pi^*$ transitions due to C═O and the conjugated C═C band, respectively.[29] Figure 4a shows the UV−vis absorption spectra of Mn NF, Mn NF + NR, and Mn NR in which a broad peak ranging from 250 to 500 nm overlaps with the emission spectrum of Cdots. This result confirms that the FRET mechanism occurs between electron-donor Cdots and different shapes of the electron-acceptor MnO_2 nanostructure. It was also found that the overlap region of the Cdot-MnO_2 nanostructure becomes maximum in the Mn−NF shape and minimum in the Mn-NR shape. From this result, it can be concluded that different shapes of the MnO_2 nanostructure play a different role in the FRET mechanism between Cdots and the MnO_2 nanostructure.

The spectral overlap integral $[J(\lambda)]$ values between Cdots and MnO_2 nanostructures were evaluated by using the ensuing equation

$$J(\lambda) = \frac{\int_0^\infty F_D(\lambda)\varepsilon_A(\lambda)\lambda^4 D\lambda}{\int_0^\infty F_D(\lambda)d\lambda} \quad (2)$$

where "$F_D(\lambda)$" corresponds to the normalized PL intensity of the electron-rich Cdots with the range of wavelengths $\lambda + d\lambda$ and "$\varepsilon_A(\lambda)$" represents the molar extinction coefficient of the electron-deficient MnO_2 nanostructure. We observed from the values of $J(\lambda)$ and also from Figure 4a that the variation in the shape of the MnO_2 nanostructure from Mn NF to Mn NR leads to a decrease in the spectral overlap integral.

Figure 4b shows BET N_2 adsorption−desorption curves for the different shapes of the MnO_2 nanostructure (Mn NF, Mn NF + NR, and Mn NR), and these curves showed the Type IV adsorption isotherm that indicates the mesoporous nature. The specific surface areas of each shape of the MnO_2 nanostructure, that is, Mn NF, Mn NF + NR, and Mn NR, were observed as

https://doi.org/10.1021/acsabm.1c00353
ACS Appl. Bio Mater. 2021, 4, 5158−5168

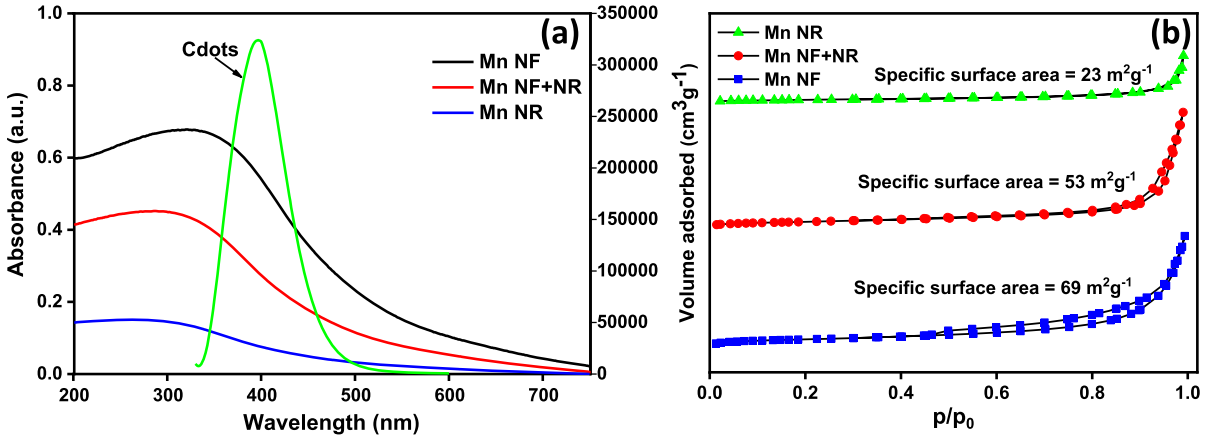

Figure 4. (a) Spectral overlap between the UV−vis absorption spectra of different MnO_2 nanostructures and the emission spectra of Cdots and (b) BET N_2 adsorption−desorption isotherms of different MnO_2 nanostructures.

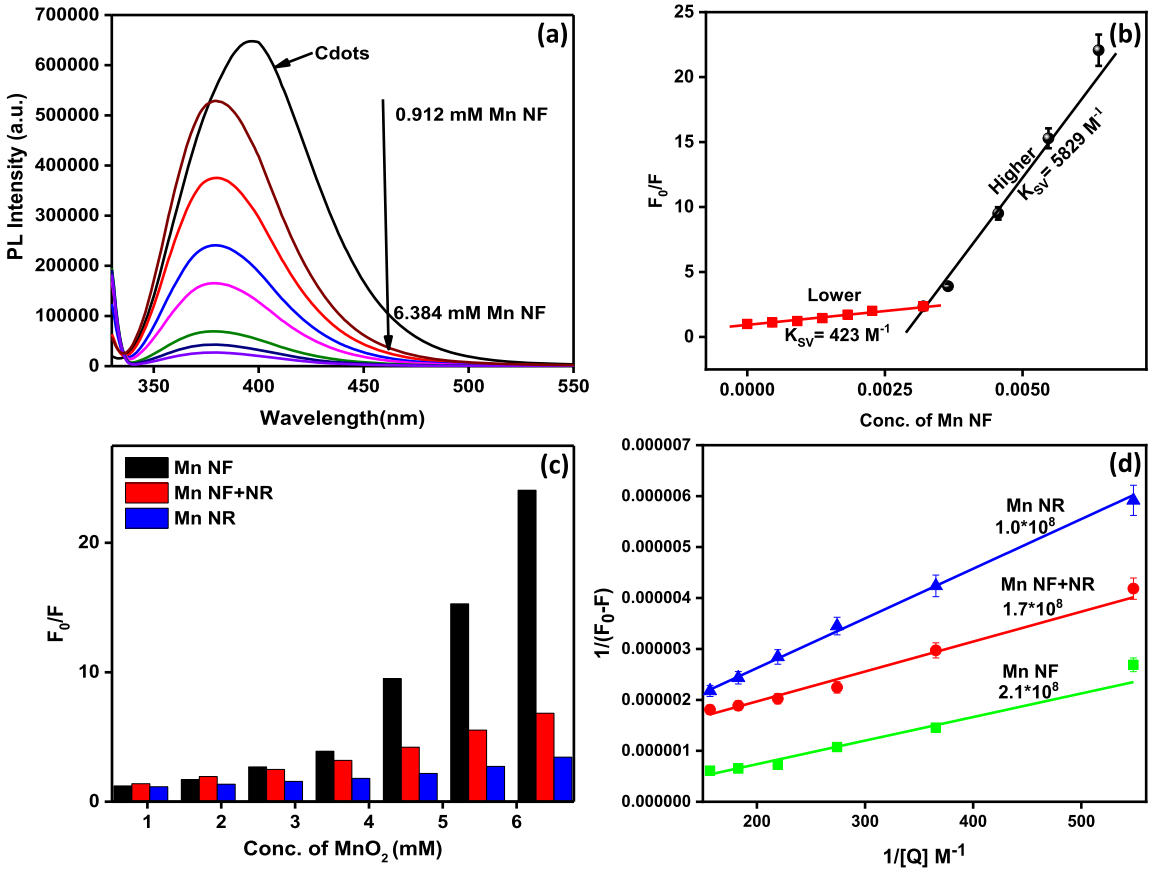

Figure 5. (a) Spectra of fluorescence quenching of Cdots with the addition of consecutive amounts of Mn NF, (b) Stern−Volmer quenching plot of different MnO_2 nanostructures with Cdots, (c) bar graph of fluorescence quenching efficiency of different shapes of the MnO_2 nanostructure at various concentrations, and (d) B−H binding plot of different MnO_2 nanostructures with Cdots.

69, 53, and 23 $m^2\ g^{-1}$, respectively. The specific surface areas, total pore volumes, and mean pore diameters of different shapes of MnO_2 nanostructures are mentioned in Table S1. Mn NF showed the maximum specific surface area that results in a large number of active sites present on its surface and provides a high charge-transfer rate.

Quenching of Fluorescence of Cdots by Different MnO_2 Nanostructures. The FRET mechanism of the Cdot-MnO_2 nanostructure was also confirmed by the fluorescence quenching study.[15,31] The prepared Cdots showed high fluorescence intensity, which was effectively quenched with the addition of different shapes of the MnO_2 nanostructure. The level of quenching of the Cdots was different in the presence of different shapes of the MnO_2 nanostructure. The mechanism of fluorescence quenching of Cdots is based on holes and electrons which get trapped in Cdots and the MnO_2 nanostructure and result in low availability used for radiative recombination.[34] The different concentrations of the MnO_2 nanostructure were varied from 0.912 to 6.384 mM for investigating the fluorescence quenching of Cdots. We

https://doi.org/10.1021/acsabm.1c00353
ACS Appl. Bio Mater. 2021, 4, 5158−5168

Table 1. Photophysical Parameters of Cdots with Different Shapes of MnO_2 Nanostructures and GSH[a]

systems	Φ	τ_{av} (ns)	k_r ($10^9 s^{-1}$)	k_{nr} ($10^9 s^{-1}$)	k_{ET} ($10^9 s^{-1}$)	Φ_{EET} (τD)	Φ_{EET} (ΦD)
Cdots	0.68	4.40	0.15	0.07			
Cdots + Mn NF	0.07	1.26	0.04	0.74	0.57	0.71	0.89
Cdots + Mn NF + GSH	0.35	3.85	0.09	0.16	0.03	0.12	0.49
Cdots + Mn (NF + NR)	0.10	2.33	0.05	0.38	0.20	0.47	0.85
Cdots + Mn (NF + NR) + GSH	0.30	3.76	0.08	0.19	0.04	0.14	0.56
Cdots + Mn NR	0.25	3.55	0.07	0.21	0.06	0.19	0.63
Cdots + Mn NR + GSH	0.33	3.86	0.09	0.17	0.03	0.12	0.52

[a]Experimental error ±5%.

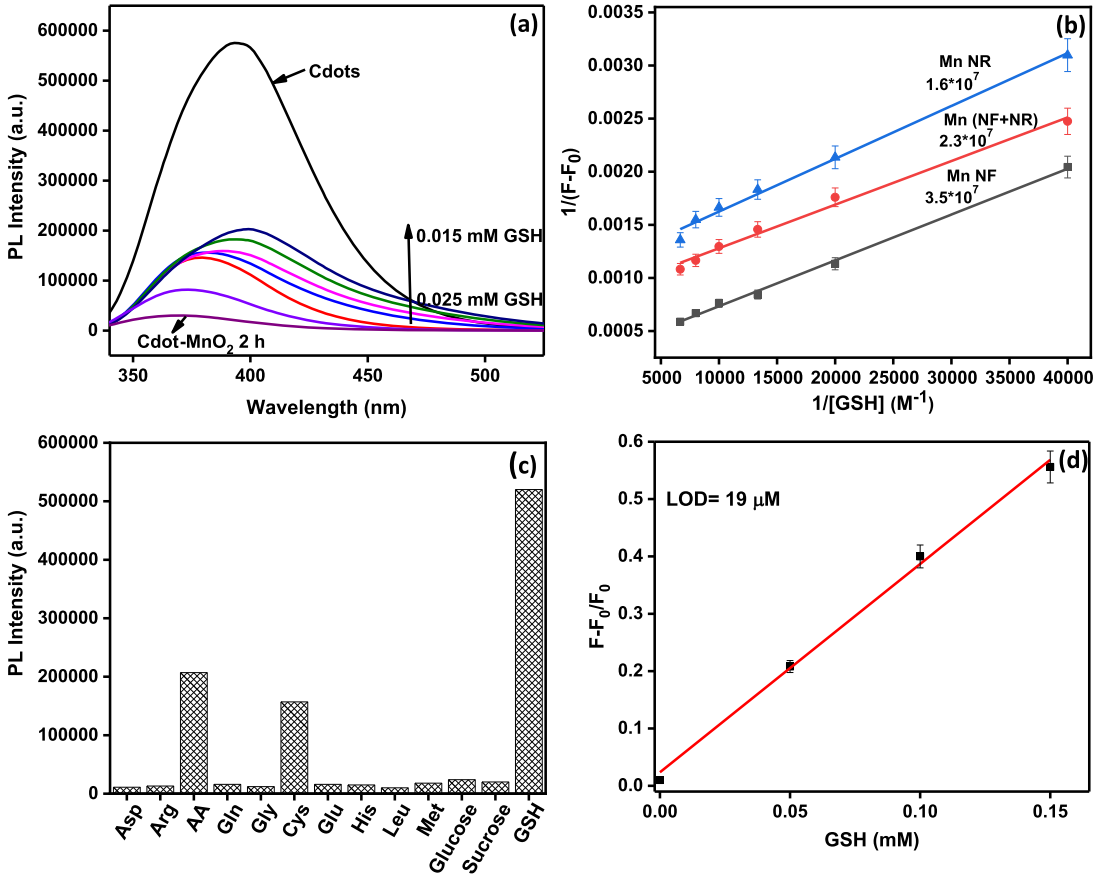

Figure 6. (a) Fluorescence recovery of the Cdot-Mn NF sensing probe with the successive addition of 50 μL of GSH (1 mM); (b) B−H binding plot of Mn NF, Mn NF + NR, and Mn NR with GSH; (c) fluorescence response of the Cdot-MnO_2 nanostructure as a sensing system toward different species; and (d) plot of fluorescence responses of the Cdot-Mn NF system $[(F - F_0)/F_0]$ vs GSH concentration.

observed that the fluorescence intensity of Cdots was quenched by different MnO_2 nanostructures up to a 6.384 mM concentration, as shown in Figures 5a and S1a,c. To figure out the level of quenching efficiency by different shapes of quenchers [Q], we have plotted the graph between F_0/F and the concentration of Q based on the resulting Stern−Volmer equation

$$\frac{F_0}{F} = 1 + K_{SV}[Q] \tag{3}$$

where "F_0" and "F" correspond to the fluorescence intensity of Cdots in the absence and presence of Q (i.e., the MnO_2 nanostructure), respectively. The Stern−Volmer quenching constant is represented as K_{SV}. The plot between F_0/F and the concentration of different Q, that is, Mn NF, Mn NF + NR, and Mn NR, is shown in Figures 5b and S1b,d, respectively. From the slope values of these plots, we have evaluated the K_{SV} value of the respective shape of the MnO_2 nanostructure. Cdots show two different K_{SV} values, which are 423 and 5829 M^{-1}, respectively, at lower- and higher-concentration regions of Mn NF as a quencher. In the case of Mn NF + NR and Mn NR, the K_{SV} values were estimated as 656 and 264 M^{-1}, respectively. Therefore, the extent of quenching efficiency of Cdots follows the order of Mn NF > Mn NF + NR > Mn NR. It can be seen in Figure 5c that Mn NF showed a significant increment in F_0/F value as the concentration of Q increases as compared to the other shapes, that is, Mn NF + NR and Mn NR. Mn NF has a larger specific surface area (69 $m^2 g^{-1}$) as well as a high pore volume (0.374 $cm^3 g^{-1}$) compared to other shapes of the MnO_2 nanostructure (23 and 53 $m^2 g^{-1}$) represented in Figure 4b and Table S1. The normal open structure of Mn NF reduces the transport distance between electrons and cations, and they showed the maximum quenching because of having a huge surface area and a

https://doi.org/10.1021/acsabm.1c00353
ACS Appl. Bio Mater. 2021, 4, 5158−5168

Table 2. Comparative Table of LOD Values for GSH by Using Different Sensing Probes and Techinques

sensing probe	technique	detection range	LOD	refs
AuNCs@BSA-MnO_2NSs	fluorescence	0−0.5 mM	20 μM	38
Ag_2SQD/MnO_2 NS	fluorescence	0.3−1.2 mM	60 μM	39
CoOOH NSs	colorimetric	33 μM−1.3 mM	13.7 μM	40
naphthalene derivative containing piazselenole (NDP)	colorimetric	0−80 mM	0.178 mM	41
cobalt phthalocyanine (CoPc) and multiwalled carbon NTs functionalized with carboxyl groups (MWCNTf)	differential pulse voltammetry	0.5−7 mM	100 μM	42
Cdot-MnO_2 NFs	fluorescence	0.0−0.15 mM	19 μM	present work

reduced amount of charge-transfer resistance.[17] Therefore, it can be said that the variation in the surface area and pore structure of MnO_2 plays a vital role and significantly alters the variation of electron-transfer rate in the excited state of Cdots. On the other hand, we can also demonstrate that the electron-transfer rate from Cdots (electron-rich) to the MnO_2 nanostructure (electron-deficient) gradually decreases as the shape changes from Mn NF to Mn NR.

Further, to comprehend the nature of stoichiometry and interaction among Cdots and various shapes of MnO_2 nanostructures, the excited-state binding constant values have been estimated by using their respective fluorescence intensity data using the 1:1 linear Benesi−Hildebrand equation[35]

$$\frac{1}{F_0 - F} = \frac{1}{F_0 - F_1} + \frac{1}{K[Q](F_0 - F)} \quad (4)$$

where "F_0" and "F" are the fluorescence intensities in the absence and presence of different shapes of MnO_2 nanostructures. "Q" represents the quencher's concentration. "F_1" corresponds to the fluorescence intensity for 1:1 stoichiometric Cdot-MnO_2 nanocomposites. The parameter "K" corresponds to the values of binding constant of Cdots and various shapes of MnO_2 nanostructures. The plot between $(1/F - F_0)$ against $1/[Q]$ gives a straight line for all shapes of the MnO_2 nanostructure (Figure 5d). From this plot, we have estimated the binding constant values (K) of Cdots, which are 2.1×10^8, 1.7×10^8, and 1×10^8 M^{-1} in the presence of Mn NF, Mn NF + NR, and Mn NR, respectively. From these data, we observed that the binding constant values gradually decrease as the shape of the MnO_2 nanostructure changes from Mn NF to Mn NR. Therefore, it can be demonstrated that the variation in the shape of the MnO_2 nanostructure had an impact on their interaction or electron transfer with Cdots, which results in deviation in the value of the binding constant of Cdots. Mn NF showed the maximum value of binding constant for Cdots due to large quantity of active sites on its surface (due to a high surface area) as compared to other shapes of MnO_2 nanostructures. It can be demonstrated that electrons get transferred easily from Cdots (donor) to Mn NF (acceptor) as compared to the other two shapes.

The values of fluorescence quantum yield (Φ) of Cdots with various systems were evaluated by using eq 1 and are tabulated in Table1. We found that the values of Φ for Cdots are considerably quenched with the addition of specific concentrations of different shapes of the MnO_2 nanostructure. The fluorescence quantum yields of Cdots are quenched ~9.7, ~6.8, and ~2.7 times in the presence of Mn NF, Mn NF + NR, and Mn NR, respectively. As a result, the extent of Φ value of Cdots follows the trend of Mn NF > Mn NF + NR > Mn NR.

Fluorescence Recovery of Cdots and GSH Determination. The addition of GSH in different shapes of the MnO_2 nanostructure, that is, Mn NF, Mn NF + NR, and Mn NR, leads to recovery of fluorescence (turn-on) of Cdots which was observed in Figures 6a and S2a,c, respectively. The restoration of fluorescence of Cdots depends upon the redox reaction among the MnO_2 nanostructure and GSH by the following equation:

$$2GSH + MnO_2 + 2H^+ \rightarrow GSSG + Mn^{2+} + 2H_2O \quad (5)$$

In the above reaction, MnO_2 gets converted to Mn^{2+} in the presence of GSH and itself gets oxidized to GSH disulfide (GSSG).[36] This results in the exclusion of Cdots from the huge surface of the MnO_2 nanostructure and leads to the recovery of fluorescence of Cdots. Cdots, MnO_2 nanostructures, and GSH play a significant role as a fluorometric reporter, quencher, and detector in this prepared sensing probe. The prepared Cdot-MnO_2 nanocomposites were used as sensing nanoprobes for GSH detection in which different concentrations of GSH were mixed with specific concentrations (6.384 mM) of different shapes of the MnO_2 nanostructure (Mn NF, Mn NF + NR, and Mn NR). It was determined that the fluorescence intensity of the Cdot-MnO_2 nanostructure enhances with the increase in the concentration of GSH. The binding constant values of the Cdot-MnO_2 nanostructure with the addition of GSH were evaluated through the Benesi−Hildebrand method.[35] It has been observed that the addition of GSH considerably changes the values of binding constant for Cdots, which are 3.5×10^7, 2.3×10^7, and 1.6×10^7 M^{-1} in the case of Mn NF, Mn NF + NR, and Mn NR, respectively (Figure 6b). The decrease in the values of binding constants of Cdots in the presence of GSH confirmed the elimination of Cdots from the surface of MnO_2 nanostructures in the order of Mn NF > Mn NF + NR > Mn NR. The fluorescence intensity of Cdots gets more recovered with the addition of GSH in the case of Mn NF as compared to other shapes of the MnO_2 nanostructure, probably because of the larger specific surface area and mesoporous nature of Mn NF. The variation in the shape of the MnO_2 nanostructure in the developed sensing nanoprobe affects the restoration (turn-on) of fluorescence of Cdots.

We also evaluated the values of fluorescence quantum yield (Φ) of different shapes of the Cdot-MnO_2 nanostructure in the presence of GSH (Table 1). For different shapes of the MnO_2 nanostructure, the fluorescence quantum yield (Φ) restorations of Cdots with the specific amount of GSH are ~5 (Mn−NF), ~3 (Mn−NF + NR), and ~1.3 (Mn-NR) times. The recovery of fluorescence of Cdots follows the trend of Mn NF > Mn NF + NR > Mn NR. This result clarified that the change in the shapes of the MnO_2 nanostructure from Mn NF to Mn NR in the Cdot-MnO_2 nanoprobe results in less efficient elimination of Cdots from the surface of MnO_2. Hence, a

https://doi.org/10.1021/acsabm.1c00353
ACS Appl. Bio Mater. 2021, 4, 5158−5168

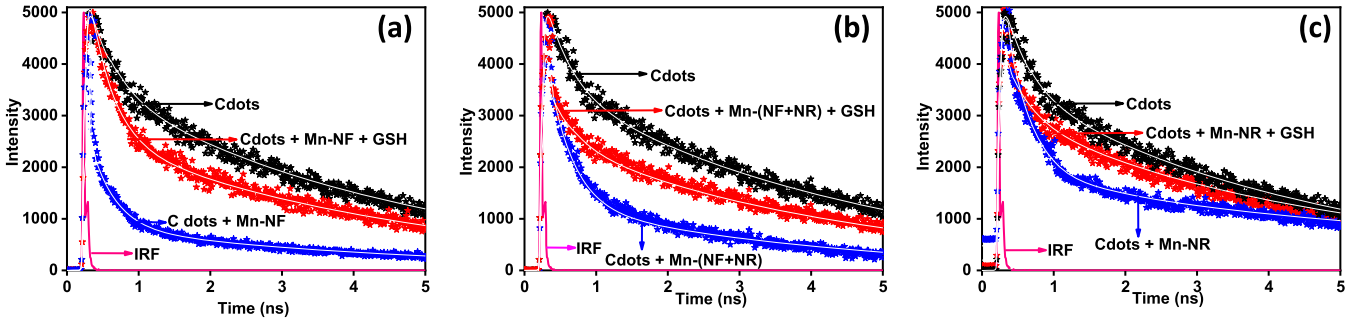

Figure 7. Fluorescence lifetime decays of Cdots in (a) Mn NF, (b) Mn (NF + NR), and (c) Mn NR and in the presence of GSH.

strong redox reaction takes place among Mn NF and GSH as compared to other shapes.

Selectivity and Sensitivity Studies. The fluorescence studies were performed with different amino acids to interpret that the developed sensing platform is selective for GSH. A particular concentration of different amino acids such as aspartic acid (Asp), arginine (Arg), ascorbic acid (AA), glutamine (Gln), glycine (Gly), cysteine (Cys), glutamic acid (Glu), histidine (His), leucine (Leu), methionine (Met), GSH, and glucose and sucrose was mixed with different Cdot-MnO_2 systems. We found that GSH showed a significant response as compared to other species (Figure 6c). It showed that different shapes of Cdot-MnO_2 nanostructures showed extreme selectivity and sensitivity for the detection analysis of GSH.

A fine linear range of the plot between $(F - F_0/F_0)$ and [GSH] was found for all three different shapes of the MnO_2 nanostructure in which F_0 and F are represented as the fluorescence intensities in the absence and presence of GSH, respectively.[37] It was found that Mn NF, Mn NF + NR, and Mn NR corresponded to distinct values of the limit of detection (LOD), that is, 19, 23, and 42 μM, respectively (Figures 6d and S2b,d). We observed the best LOD value for Mn NF in comparison with Mn NF + NR and Mn NR. Table 2 lists the LOD values for the detection of GSH by using different sensing platforms and techniques reported in the literature. These studies showed that our sensing platform and technique are simple, cheap, and green as compared to other expensive sensing platforms and different techniques.

Time-Resolved Emission Studies. To get more insight into the interaction of different shapes of the Cdot-MnO_2 nanostructure and their impact on the detection of GSH, we have performed fluorescence time-resolved emission studies by exciting the respective samples at an excitation wavelength of 340 nm (λ_{exi} = 340 nm) with their respective emission wavelengths. An average lifetime (τ_{av}) value of prepared Cdots is 4.40 ns, and the addition of a specific amount of different shapes of the MnO_2 nanostructure leads to significant variation in quenching of the values of lifetime decay of Cdots (Figure 7). From Table 1, it was found that the average lifetime values of Cdots were quenched 71, 47, and 19% in the presence of Mn NF, Mn NF + NR, and Mn NR, respectively. From this analysis, it is confirmed that Cdots show maximum quenching in the presence of Mn NF while minimum in Mn NR. Astonishingly, in the presence of GSH as a sensing agent, the average lifetime values of different shapes of the Cdot-MnO_2 nanostructure showed an increment of their respective lifetime values. This result confirms that Cdots exhibited recovery (turn-on) of fluorescence with the particular amount of GSH. The increment of the lifetime of Cdots in the presence of GSH is solely dependent on different shapes of the MnO_2 nanostructure. The fluorescence restorations (turn-on) of Cdots in the presence of GSH were found to be 67, 38, and 8% for Mn NF, Mn NF + NR, and Mn NR, respectively.

To rationalize the clear idea on excited-state dynamics of Cdots, we have calculated the rate of electron transfer (k_{ET}) in the presence of different shapes of the MnO_2 nanostructure and also in the presence of GSH by using eq 6

$$k_{ET} = \frac{1}{\tau_{DA}} - \frac{1}{\tau_D} \tag{6}$$

where "τ_D" and "τ_{DA}" correspond to the values of average lifetime of Cdots in the absence and presence of the MnO_2 nanostructure, respectively. The electron-transfer rate considerably changes with the variation in shapes of the MnO_2 nanostructure. From Table 1, it was found that the electron-transfer rate from electron-donor Cdots to different shapes of the electron-acceptor MnO_2 nanostructure followed the order of Mn−NF > Mn−NF + NR > Mn NR. This result confirms that the electron-transfer process of Cdots solely depends on the shape of the MnO_2 nanostructure. Moreover, the existence of GSH results as interruption of the electron-transfer process of Cdots as GSH shows redox reaction with the MnO_2 nanostructure. This results as release of Cdots from the surface of the MnO_2 nanostructure. The electron-transfer efficiency (Φ_{EET}) is estimated by the following equation:

$$\Phi_{EET} = 1 - \frac{\phi_{DA}}{\phi_D} = 1 - \frac{\tau_{DA}}{\tau_D} \tag{7}$$

The parameters "Φ_D" and "Φ_{DA}" represent quantum yields of Cdots in the absence and presence of different shapes of the MnO_2 nanostructure, respectively. The calculated values of EET (Table 1) by using both the values of quantum yield [Φ_{EET} (Φ_D)] and lifetime [Φ_{EET} (τ_D)] also signify that the electron-transfer efficiency for Cdots considerably changes and depends on the shapes of the MnO_2 nanostructure, which follows the order of Mn NF > Mn NF + NR > Mn NR. Moreover, the presence of GSH diminishes [Φ_{EET} (Φ_D)] and [Φ_{EET} (τ_D)] values of Cdots, which approves that the presence of GSH results as exclusion of Cdots from the MnO_2 nanostructure's surface.

We have further estimated radiative (k_r) and nonradiative (k_{nr}) rate constant values via eqs 8 and 9

$$k_r = \frac{\phi_f}{\tau_f} \tag{8}$$

$$\frac{1}{\tau_f} = k_r + k_{nr} \tag{9}$$

https://doi.org/10.1021/acsabm.1c00353
ACS Appl. Bio Mater. 2021, 4, 5158−5168

The k_r and k_{nr} values are tabulated in Table1. We found that the k_{nr} values of Cdots get increased by 10.5, 5.4, and 3 times, whereas the values of k_r decreased by 0.26, 0.33, and 0.46 times, respectively, in the existence of Mn NF, Mn NF + NR, and Mn NR. The decrease of k_r values and the increase of k_{nr} values of Cdots confirm that Cdots get less fluorescence in the presence of different shapes of the MnO_2 nanostructure (maximum for Mn−NF and minimum for Mn-NR). Further, it was found that the presence of GSH to the Cdot-MnO_2 system considerably increases k_r values and decreases k_{nr} values, which confirms that GSH has the propensity to drive out Cdots from different shapes of the MnO_2 nanostructure. Finally, we observed fluorescence restoration (turn-on), which implies that Cdots get more fluorescence in GSH. We have estimated the FRET efficiency (E) of Cdots with the addition of different shapes of the MnO_2 nanostructure by using the following equation:[43]

$$E = \frac{k_{ET}}{k_r + k_{ET} + k_{nr}} \tag{10}$$

It was found from Table 3 that "E" of Cdots exclusively depends on the variant shapes of the MnO_2 nanostructure,

Table 3. Förster Distance (R_0), Efficiency Percentage (E %), and Separation Distance (r) of Different Cdot-MnO_2 Systems

systems	R_0 (Å)	E (%)	r (nm)
Cdots			
Cdots + Mn NF	4.97	42	1.53
Cdots + Mn NF + NR	8.50	32	2.95
Cdots +Mn NR	12.52	18	6.14

which follows the order of Mn NF > Mn NF + NR > Mn NR. This result confirms that the FRET mechanism of Cdots is more pronounced in Mn NF as compared to other shapes.

Furthermore, we also determined the Förster distance (R_0) between Cdots and different shapes of MnO_2 nanostructures through the following equation:[43]

$$R_0 = 0.211[\kappa^2 \eta^{-4} \Phi_D J(\lambda)]^{1/6} \tag{11}$$

"R_0" is the distance between the center of the donor (Cdots) and the center of the acceptor (MnO_2 nanostructure). The relative orientation factor is denoted by κ^2 for the transition dipoles of the donor and the acceptor in isotropic solution. The other parameters "η", "Φ_D", and "$J(\lambda)$" are represented as the viscosity of the medium, the fluorescence quantum yield of the donor (Cdots), and the spectral overlap integral, respectively. The calculated R_0 values are tabulated in Table 3, which approves that the interaction among Cdots and different shapes of the nanostructure fulfills the classical FRET theory.[43] Further, we have also calculated the separation distance (r) between the different shapes of the MnO_2 nanostructure and Cdots by using the following equation:[43]

$$E = \frac{1}{1 + \left(\frac{r}{R_0}\right)^6} \tag{12}$$

The separation distance (r) between the different shapes of the MnO_2 nanostructure and Cdots steadily increases with the variation in the shape of the MnO_2 nanostructure from Mn NF to Mn NR (1.53, 2.95, and 6.14 nm for Mn NF, Mn NF + NR, and Mn NR, respectively). Mn NF has the shortest separation distance with Cdots as compared to other shapes, which confirms that the Mn NF has the maximum FRET efficiency.

CONCLUSIONS

The fluorescent and highly water-soluble Cdots were synthesized using ascorbic acid (carbon source) via the bottom-up approach including microwave irradiation. The role of different morphologies (shapes) of the MnO_2 nanostructure in the fluorescence sensing system based on the Cdot-MnO_2 nanostructure for GSH sensing was studied in detail. The specific surface area of different MnO_2 structures is determined by BET and follows the order of Mn NF > Mn NF + NR > Mn NR. Mn NF showed maximum fluorescence quenching of Cdots and a higher value of Stern−Volmer quenching constants (K_{SV}) due to the high specific surface area and the high electron-transfer rate (k_{ET}). There was a decrease in the values of fluorescence quantum yield (Φ) and average lifetime [τ_{av} (ns)], which confirms the occurrence of the FRET mechanism from Cdots (electron donor) to Mn NF (electron acceptor). The calculated values of FRET efficiency (E) confirmed that the maximum FRET occurs in the case of Mn NF. The electron-transfer efficiency was calculated utilizing the values of both quantum yield [Φ_{EET} (Φ_D)] and lifetime [Φ_{EET} (τ_D)], and it was higher in the case of Mn NF. The decrease in radiative (k_r) and increase in nonradiative (k_{nr}) rate constants showed that the Cdots get less fluorescence in the presence of different shapes of the MnO_2 nanostructure (maximum for Mn NF and minimum for Mn NR). The prepared sensing systems showed fluorescence recovery of Cdots due to the occurrence of redox reaction between GSH and MnO_2, which results in the conversion of MnO_2 to Mn^{2+}. The highest LOD (19 μM) for GSH was observed in the case of Cdot-Mn NF sensing systems. Hence, the variation in the morphology of the MnO_2 nanostructure in the developed sensing system had a great impact on the sensing of GSH.

ASSOCIATED CONTENT

Supporting Information

The Supporting Information is available free of charge at https://pubs.acs.org/doi/10.1021/acsabm.1c00353.

Surface specifications of different shapes of MnO_2 nanostructures; fluorescence quenching of Cdots with different concentrations of Mn NF + NR and Mn NR and their Stern−Volmer quenching plots; and fluorescence restoration of Cdot-Mn NF + NR/Mn NR in the presence of GSH and their linear relationship between fluorescence responses with different concentrations of GSH (PDF)

AUTHOR INFORMATION

Corresponding Authors

Banibrata Maity − *School of Chemistry and Biochemistry, Affiliate Faculty-TIET-Virginia Tech Center of Excellence in Emerging Materials, Thapar Institute of Engineering and Technology, Patiala 147004, India;* orcid.org/0000-0003-0286-9028; Email: banibrata.maity@thapar.edu

Soumen Basu − *School of Chemistry and Biochemistry, Affiliate Faculty-TIET-Virginia Tech Center of Excellence in Emerging Materials, Thapar Institute of Engineering and Technology, Patiala 147004, India;* orcid.org/0000-0001-6419-1326; Email: soumen.basu@thapar.edu

https://doi.org/10.1021/acsabm.1c00353
ACS Appl. Bio Mater. 2021, 4, 5158−5168

Author

Neeraj Sohal − *School of Chemistry and Biochemistry, Thapar Institute of Engineering and Technology, Patiala 147004, India;* orcid.org/0000-0002-3737-0932

Complete contact information is available at: https://pubs.acs.org/10.1021/acsabm.1c00353

Notes

The authors declare no competing financial interest.

■ ACKNOWLEDGMENTS

The authors would like to thank CSIR [grant no: 01 (2955)/18/EMR-II] for funding and fellowship. Also, the authors are grateful to the Centre for Nano and Soft Matter Sciences (CeNS), Bengaluru, for HR-TEM analysis.

■ REFERENCES

(1) Zhang, S.; Ong, C.-N.; Shen, H.-M. Critical Roles of Intracellular Thiols and Calcium in Parthenolide-Induced Apoptosis in Human Colorectal Cancer Cells. *Canc. Lett.* **2004**, *208*, 143−153.

(2) Pan, J.; Zheng, Z.; Yang, J.; Wu, Y.; Lu, F.; Chen, Y.; Gao, W. A Novel and Sensitive Fluorescence Sensor for Glutathione Detection by Controlling the Surface Passivation Degree of Carbon Quantum Dots. *Talanta* **2017**, *166*, 1−7.

(3) Li, R.; Kassaye, H.; Pan, Y.; Shen, Y.; Li, W.; Cheng, Y.; Guo, J.; Xu, Y.; Yin, H.; Yuan, Z. A Visible and Near-Infrared Dual-Fluorescent Probe for Discrimination between Cys/Hcy and GSH and Its Application in Bioimaging. *Biomater. Sci.* **2020**, *8*, 5994−6003.

(4) Yan, X.; Song, Y.; Zhu, C.; Song, J.; Du, D.; Su, X.; Lin, Y. Graphene Quantum Dot-MnO2 Nanosheet Based Optical Sensing Platform: A Sensitive Fluorescence "Turn Off-On" Nanosensor for Glutathione Detection and Intracellular Imaging. *ACS Appl. Mater. Interfaces* **2016**, *8*, 21990−21996.

(5) Song, Z.-L.; Dai, X.; Li, M.; Teng, H.; Song, Z.; Xie, D.; Luo, X. Biodegradable Nanoprobe Based on MnO2 Nanoflowers and Graphene Quantum Dots for near Infrared Fluorescence Imaging of Glutathione in Living Cells. *Microchim. Acta* **2018**, *185*, 485.

(6) Yang, Y.; Zhao, Q.; Feng, W.; Li, F. Luminescent Chemodosimeters for Bioimaging. *Chem. Rev.* **2013**, *113*, 192−270.

(7) Ji, C.; Zhou, Y.; Leblanc, R. M.; Peng, Z. Recent Developments of Carbon Dots in Biosensing: A Review. *ACS Sens.* **2020**, *5*, 2724−2741.

(8) Bhattacharya, S.; Sarkar, R.; Chakraborty, B.; Porgador, A.; Jelinek, R. Nitric Oxide Sensing through Azo-Dye Formation on Carbon Dots. *ACS Sens.* **2017**, *2*, 1215−1224.

(9) Fong, J. F. Y.; Chin, S. F.; Ng, S. M. A Unique "Turn-on" Fluorescence Signalling Strategy for Highly Specific Detection of Ascorbic Acid Using Carbon Dots as Sensing Probe. *Biosens. Bioelectron.* **2016**, *85*, 844−852.

(10) Pandit, S.; Banerjee, T.; Srivastava, I.; Nie, S.; Pan, D. Machine Learning-Assisted Array-Based Biomolecular Sensing Using Surface-Functionalized Carbon Dots. *ACS Sens.* **2019**, *4*, 2730−2737.

(11) Li, M.; Chen, T.; Gooding, J. J.; Liu, J. Review of Carbon and Graphene Quantum Dots for Sensing. *ACS Sens.* **2019**, *4*, 1732−1748.

(12) Kainth, S.; Maity, B.; Basu, S. Deciphering the Interaction of Solvents with Dual Emissive Carbon Dots: A Photoluminescence Study and Its Response for Different Metal Ions. *Mater. Sci. Eng. C* **2020**, *108*, 110443.

(13) Zu, F.; Yan, F.; Bai, Z.; Xu, J.; Wang, Y.; Huang, Y.; Zhou, X. The Quenching of the Fluorescence of Carbon Dots: A Review on Mechanisms and Applications. *Microchim. Acta* **2017**, *184*, 1899−1914.

(14) Tehseen, B.; Rehman, A.; Rahmat, M.; Bhatti, H. N.; Wu, A.; Butt, F. K.; Naz, G.; Khan, W. S.; Bajwa, S. Z. Solution Growth of 3D MnO2 Mesh Comprising 1D Nanofibres as a Novel Sensor for Selective and Sensitive Detection of Biomolecules. *Biosens. Bioelectron.* **2018**, *117*, 852−859.

(15) Wang, Y.; Jiang, K.; Zhu, J.; Zhang, L.; Lin, H. A FRET-Based Carbon Dot−MnO 2 Nanosheet Architecture for Glutathione Sensing in Human Whole Blood Samples. *Chem. Commun.* **2015**, *51*, 12748−12751.

(16) Garg, D.; Mehta, A.; Mishra, A.; Basu, S. A Sensitive Turn on Fluorescent Probe for Detection of Biothiols Using MnO2@carbon Dots Nanocomposites. *Spectrochim. Acta Mol. Biomol. Spectrosc.* **2018**, *192*, 411−419.

(17) Sohal, N.; Maity, B.; Shetti, N. P.; Basu, S. Biosensors Based on MnO2Nanostructures: A Review. *ACS Appl. Nano Mater.* **2021**, *4*, 2285−2302.

(18) Ede, S. R.; Anantharaj, S.; Nithiyanantham, U.; Kundu, S. DNA-Encapsulated Chain and Wire-like β-MnO2 Organosol for Oxidative Polymerization of Pyrrole to Polypyrrole. *Phys. Chem. Chem. Phys.* **2015**, *17*, 5474−5484.

(19) Wu, Y.; Deng, P.; Tian, Y.; Magesa, F.; Liu, J.; Li, G.; He, Q. Construction of Effective Electrochemical Sensor for the Determination of Quinoline Yellow Based on Different Morphologies of Manganese Dioxide Functionalized Graphene. *J. Food Compos. Anal.* **2019**, *84*, 103280.

(20) Sinha, L.; Pakhira, S.; Bhojane, P.; Mali, S.; Hong, C. K.; Shirage, P. M. Hybridization of Co 3 O 4 and α-MnO 2 Nanostructures for High-Performance Nonenzymatic Glucose Sensing. *ACS Sustain. Chem. Eng.* **2018**, *6*, 13248−13261.

(21) Yamaguchi, Y.; Aono, R.; Hayashi, E.; Kamata, K.; Hara, M. Template-Free Synthesis of Mesoporous β-MnO 2 Nanoparticles: Structure, Formation Mechanism, and Catalytic Properties. *ACS Appl. Mater. Interfaces* **2020**, *12*, 36004−36013.

(22) Pargoletti, E.; Cappelletti, G.; Minguzzi, A.; Rondinini, S.; Leoni, M.; Marelli, M.; Vertova, A. High-Performance of Bare and Ti-Doped α-MnO2 Nanoparticles in Catalyzing the Oxygen Reduction Reaction. *J. Power Sources* **2016**, *325*, 116−128.

(23) Samdani, J.; Samdani, K.; Kim, N. H.; Lee, J. H. A New Protocol for the Distribution of MnO 2 Nanoparticles on RGO Sheets and the Resulting Electrochemical Performance. *Appl. Surf. Sci.* **2017**, *399*, 95−105.

(24) Shen, H.; Huang, J.; Wei, Y.; Guo, X.; Wang, M.; Wang, L. Effect of Morphology of ϵ-MnO 2 on Hydrogen Peroxide Sensing. *ChemistrySelect* **2019**, *4*, 4035−4043.

(25) Cheng, G.; Yu, L.; He, B.; Sun, M.; Zhang, B.; Ye, W.; Lan, B. Catalytic Combustion of Dimethyl Ether over α-MnO2 Nanostructures with Different Morphologies. *Appl. Surf. Sci.* **2017**, *409*, 223−231.

(26) Ede, S. R.; Ramadoss, A.; Anantharaj, S.; Nithiyanantham, U.; Kundu, S. Enhanced Catalytic and Supercapacitor Activities of DNA Encapsulated β-MnO2 Nanomaterials. *Phys. Chem. Chem. Phys.* **2014**, *16*, 21846−21859.

(27) Peng, T.; Dai, X.; Zhang, Y.; Zheng, P.; Wang, J.; Wang, S.; Wang, Z.; Zeng, Y.; Li, J.; Jiang, H. Facile synthesis of SiO_2@MnO_2 nanocomposites and their applications on platforms for sensitively sensing antibiotics and glutathione. *Sens. Actuators, B* **2020**, *304*, 127314.

(28) Li, T.; Wang, Z.; Jiang, D.; Wang, H.; Lai, W.-F.; Lv, Y.; Zhai, Y. A FRET Biosensor Based on MnO2 Nanosphere/Copper Nanocluster Complex: From Photoluminescence Quenching to Recovery and Magnification. *Sens. Actuators, B* **2019**, *290*, 535−543.

(29) Sohal, N.; Maity, B.; Basu, S. Carbon Dot-MnO2Nanosphere Composite Sensors for Selective Detection of Glutathione. *ACS Appl. Nano Mater.* **2020**, *3*, 5955−5964.

(30) Yuan, H.; Deng, L.; Qi, Y.; Kobayashi, N.; Hasatani, M. Morphology-Dependent Performance of Nanostructured MnO2 as an Oxygen Reduction Catalyst in Microbial Fuel Cells. *Int. J. Electrochem. Sci.* **2014**, *10*, 3693−3706.

(31) He, D.; Yang, X.; He, X.; Wang, K.; Yang, X.; He, X.; Zou, Z. A Sensitive Turn-on Fluorescent Probe for Intracellular Imaging of Glutathione Using Single-Layer MnO2 Nanosheet-Quenched Fluorescent Carbon Quantum Dots. *Chem. Commun.* **2015**, *51*, 14764−14767.

(32) Crosby, G. A.; Demas, J. N. Measurement of Photoluminescence Quantum Yields. Review. *J. Phys. Chem.* **1971**, *75*, 991−1024.
(33) Su, D.; Ahn, H.-J.; Wang, G. Hydrothermal Synthesis of α-MnO2 and β-MnO2 Nanorods as High Capacity Cathode Materials for Sodium Ion Batteries. *J. Mater. Chem. A* **2013**, *1*, 4845.
(34) Mehta, A.; Mishra, A.; Kainth, S.; Basu, S. Carbon Quantum Dots/TiO2 Nanocomposite for Sensing of Toxic Metals and Photodetoxification of Dyes with Kill Waste by Waste Concept. *Mater. Des.* **2018**, *155*, 485−493.
(35) Hildebrand, J. H.; Benesi, H. A. Interaction of Iodine with Aromatic Hydrocarbons [15]. *Nature* **1949**, *164*, 963.
(36) Gao, W.; Liu, Z.; Qi, L.; Lai, J.; Kitte, S. A.; Xu, G. Ultrasensitive Glutathione Detection Based on Lucigenin Cathodic Electrochemiluminescence in the Presence of MnO2 Nanosheets. *Anal. Chem.* **2016**, *88*, 7654−7659.
(37) Li, H.; Jin, L.; Kan, Y.; Yin, B. A Visual and "Turn-on" Fluorescent Probe for Rapid Detection of Cysteine over Homocysteine and Glutathione. *Sens. Actuators, B* **2014**, *196*, 546−554.
(38) Lin, S.; Cheng, H.; Ouyang, Q.; Wei, H. Deciphering the Quenching Mechanism of 2D MnO 2 Nanosheets towards Au Nanocluster Fluorescence to Design Effective Glutathione Biosensors. *Anal. Methods* **2016**, *8*, 3935−3940.
(39) Shu, Y.; Gao, J.; Chen, J.; Yan, J.; Sun, J.; Jin, D.; Xu, Q.; Hu, X. A Near−infrared Fluorescent Sensor Based on the Architecture of Low−toxic Ag2S Quantum Dot and MnO2 Nanosheet for Sensing Glutathione in Human Serum Sample. *Talanta* **2021**, *221*, 121475.
(40) Li, J.; Jiao, L.; Xu, W.; Yan, H.; Chen, G.; Wu, Y.; Hu, L.; Gu, W. Cobalt Oxyhydroxide Nanosheets Integrating with Metal Indicator Enable Sensitive Detection of Glutathione. *Sens. Actuators, B* **2021**, *329*, 129247.
(41) Zeng, X.; Zhang, X.; Zhu, B.; Jia, H.; Yang, W.; Li, Y.; Xue, J. A Colorimetric and Ratiometric Fluorescent Probe for Quantitative Detection of GSH at Physiologically Relevant Levels. *Sens. Actuators, B* **2011**, *159*, 142−147.
(42) Moya, P. M. O.; Alfaro, M. M.; Kazemi, R.; Alpuche-Avilés, M. A.; Griveau, S.; Bedioui, F.; Granados, S. G. Simultaneous Electrochemical Speciation of Oxidized and Reduced Glutathione. Redox Profiling of Oxidative Stress in Biological Fluids with a Modified Carbon Electrode. *Anal. Chem.* **2017**, *89*, 10726−10733.
(43) Lakowicz, J. R. *Principles of Fluorescence Spectroscopy*; Lakowicz, J. R., Ed.; Springer US: Boston, MA, 2006.

https://doi.org/10.1021/acsabm.1c00353
ACS Appl. Bio Mater. 2021, 4, 5158−5168